Task 11. University of California, Berkeley (Subcontract)

The objective of this task is the characterization of the structure and function of active sites involved in the synthesis of high molecular weight hydrocarbons from CO and H_2 on multi-component catalysts based on Fe as the active component.

Table of Contents

IV. I. FISCHER-TROPSCH SYNTHESIS ON IRON CATALYSTS

1. Background

1.1. Structure and Function of Active Phases in Fischer-Tropsch Synthesis

Fe-based oxides have been used as commercial catalysts for Fischer-Tropsch synthesis (FTS) to produce a large variety of paraffin and olefin products, ranging from methane to high molecular weight waxes [1]. During activation by synthesis gas and subsequent FTS reaction, several phases including metallic iron, iron carbides and iron oxides are known to co-exist at steady-state conditions [2-5]. The distribution and amounts of these phases depend on exposure to various activation and reaction conditions, leading to different catalytic performances in FTS. Some researchers [6] have proposed that surface iron atoms are responsible for FTS activity, while others have considered surface carbides or a mixture of carbides [7,8] with metallic iron [9] to be the active phase. There are also some reports that suggest that magnetite Fe_3O_4 is the active FTS phase [10-12]. Although these studies have each provided some evidence to support their specific proposals about the active phase, the available information remains phenomenological and sometimes contradictory, and a direct method to identify the active phase during reaction and to count the number of active sites has not yet been established.

As the planned continuation of previous research on Co [13,14] and Fe catalysts [15,16] for FTS, and of our own TPSR (temperature-programmed surface reaction) studies described in the previous quarterly report using reactions of Fe oxides with H_2 and in CO, our characterization during this research period involved isothermal transient studies of Fe-based catalysts using a flowing stream of synthesis gas. We monitored the gas phase concentrations as reduction and carburization occurred using H_2/CO as reactants by means of on-line mass spectrometry, and we followed the phase evolution using *in-situ* X-ray absorption spectroscopy at the SSRL synchrotron. In this way, we have tried to establish more conclusively the active phases required for FTS. Our goal is to present a model to describe the reduction and carburization process and to refine the structure-function relationships that we have previously proposed to interpret the catalytic behavior of Fe-based catalysts.

1.2. Effects of Zn, K and Cu

Many components have been added to Fe catalysts in order to improve their mechanical and catalytic properties. Our previous studies have shown that zinc, alkali and copper [16,17] promote the catalytic properties of Fe oxides. Zinc oxide, as a non-reducible oxide in FTS conditions, appears to stabilize the surface area of Fe oxide. Alkali, as a modifier of the adsorption enthalpies of H_2 and CO, increases the selectivity to desired C_{5+} products. Copper promotes the carburization processes and decreases the temperature required for the activation of the iron oxide precursors. Here, our efforts have focused on Fe-Zn-K-Cu catalysts. We have prepared a series of Zn and Fe co-precipitated oxides with a range of Zn/Fe atomic ratios and then introduced varying amounts of K and Cu. We have examined the surface area, bulk structure, required reduction and carburization

temperatures, as well as the catalytic behavior of these catalysts, in order to identify optimum Zn/Fe ratios and Cu and K contents that give maximum site density and catalytic activity.

2. Synthesis Procedures for Fe-Zn-K-Cu Oxides

All catalysts were prepared by co-precipitation of iron and zinc nitrates (Aldrich, 99+%) at a constant pH of 7.0 in order to form porous mixed oxides. Then, these oxide precursors were impregnated with an aqueous solution of potassium carbonate (Aldrich, 99+%) and copper nitrate (Aldrich, 99+%) using incipient wetness methods. The Zn/Fe oxide precursors were prepared first. Fe nitrate (1.4 M) and Zn nitrate (3.0 M) solutions were mixed at a given Zn/Fe atomic ratio. A solution of ammonium carbonate (Aldrich, 98%) (1 M) was prepared separately. Deionized water (~ 50 ml) was added into a large flask, which was heated on a hot plate with a magnetic stirrer and held at 80 ^{o}C throughout the synthesis. The mixed Zn/Fe solution was added at 2 cm^3/min flow into the flask through a feeding pump. At the same time, the ammonium carbonate solution was fed separately, and its flow was controlled to maintain the slurry pH at 7±0.1, as monitored by a pH meter. The resulting precipitate powders were washed several times with about 1 *l* water per gram of catalyst, dried at 120 ^{o}C overnight, and then treated in dry air at 350 ^{o}C for 1 h. The air-treated material was promoted with 2 at.% K using a K_2CO_3 solution (0.16 M) and incipient wetness protocols and then dried at 373 K. A similar process was used in order to promote samples with 1 at.% Cu using $Cu(NO_3)_2$ (Aldrich, 99+%) solutions (0.16 M). Finally, the dried material was treated in dry air at 400 ^{o}C for 4 h. This final calcination temperature was chosen from temperature-programmed oxidation data, which showed that this temperature is sufficient to decompose all metal nitrates and carbonates, except K_2CO_3. The resulting catalyst precursors contain CuO, ZnO, Fe_2O_3 and K_2CO_3. These catalysts were pressed at 443 MPa into pellets, lightly crushed, and then sieved to retain the 80-140 mesh fraction used for FTS reactions and for all subsequent characterization studies.

3. Catalyst Characterization

3.1. Protocols for the Characterization of Fe-based FTS Catalysts

This research program addresses the synthesis and the structural and catalytic characterization of active sites in Fe-based catalysts for FTS. We have designed a matrix of samples that contains a systematic range of multicomponent catalysts in order to determine the number and type of surface sites present on fresh catalysts and on samples during and after FTS reaction (Table 1.1). Our objective is to develop rigorous relationships between the synthesis methods, the resulting catalyst structures, and their function in FTS reactions.

Table 1.1. Matrix of Fe-Zn-K-Cu samples and characterization methods for FTS reaction

<table>
<tr><th colspan="3">Nominal Composition of the Catalysts</th><th rowspan="2">Characterization Before and After FTS</th><th rowspan="2">FTS reaction</th></tr>
<tr><th>Zn/Fe mole ratio</th><th>K/(Fe+Zn) (at.%)</th><th>Cu/(Fe+Zn) (at.%)</th></tr>
<tr><td rowspan="6">0</td><td rowspan="2">0</td><td>0</td><td rowspan="19">XRD

Surface area

In-situ XAS

H_2-TPR

CO-TPR</td><td rowspan="19">Effect of reaction condition

220 ^oC
21.4 atm

235 ^oC
21.4 atm

270 ^oC
5 atm

Effect of CO_2 addition

Isotopic studies</td></tr>
<tr><td>1</td></tr>
<tr><td rowspan="3">2</td><td>0</td></tr>
<tr><td>1</td></tr>
<tr><td>2</td></tr>
<tr><td>4</td><td>1</td></tr>
<tr><td rowspan="3">0.05</td><td>0</td><td>0</td></tr>
<tr><td>2</td><td>1</td></tr>
<tr><td>4</td><td>2</td></tr>
<tr><td rowspan="6">0.1</td><td rowspan="2">0</td><td>0</td></tr>
<tr><td>1</td></tr>
<tr><td rowspan="3">2</td><td>0</td></tr>
<tr><td>1</td></tr>
<tr><td>2</td></tr>
<tr><td>4</td><td>1</td></tr>
<tr><td rowspan="3">0.2</td><td>0</td><td>0</td></tr>
<tr><td>2</td><td>1</td></tr>
<tr><td>4</td><td>2</td></tr>
<tr><td rowspan="6">0.4</td><td rowspan="2">0</td><td>0</td></tr>
<tr><td>1</td></tr>
<tr><td rowspan="3">2</td><td>0</td></tr>
<tr><td>1</td></tr>
<tr><td>2</td></tr>
<tr><td>6</td><td>1</td></tr>
</table>

3.2. Isothermal Switch Transient Studies of Fe-Cu-K Oxides in Synthesis Gas

A rapid switch transient method using on-line mass spectrometric detection was developed in order to determine the initial reduction and carburization behavior of Fe oxides, as well as their catalytic CO hydrogenation properties in H_2/CO mixtures. Typically, samples (0.2 g) were pretreated in dry air (100 cm^3/min) at temperatures up to 573 K and cooled down in He to 523 K. The He stream was switched to a flow of 60 % synthesis gas (H_2/CO=2) in Ar (total flow rate 100 cm^3/min) at 523 K. The resulting isothermal transients of CH_4, H_2O and CO_2 were monitored as a function of time by on-line mass spectrometry.

Accurate measurement of multiple species with overlapping mass fragments requires deconvolution of the complex product mass spectrum. Mass intensities were represented by:

$$\begin{bmatrix} I_1 \\ \mathrm{M} \\ I_N \end{bmatrix} = \left\{ \begin{bmatrix} M_{1,1} & \mathrm{K} & M_{1,K} \\ \mathrm{M} & \mathrm{O} & \\ M_{N,1} & & M_{N,K} \end{bmatrix} \cdot \left(\begin{bmatrix} R_1 \\ \mathrm{M} \\ R_N \end{bmatrix} \cdot \overline{\overline{I}} \right) \right\} \cdot \begin{bmatrix} X_1 \\ \mathrm{M} \\ X_K \end{bmatrix}$$

where I_j is the measured intensity of a fragment with mass j, $M_{j,k}$ is the relative intensity of mass j within the fragmentation pattern of species k, R_k is the intensity response of species k relative to an internal standard, I is the identity matrix, and X_k is the mole fraction of species k. The response factor is defined as:

$$R_k = \frac{I_k^*}{I_{40}} \cdot \frac{X_{Ar}}{X_k}$$

where I^*_k is the intensity of the most intense mass fragment of species k. The matrix $M_{j,k}$ was developed from experimental mass fragmentation patterns for pure species, normalized by the intensity of the most intense mass fragment. The values for $M_{j,k}$ and R_k measured with our mass spectrometer are given in

The mole fractions of the product mixture were then calculated from the experimental mass spectra using the inverse of the mass fragmentation matrix:

$$\overline{X} = \left[\overline{\overline{M}} \cdot \left(\overline{R} \cdot \overline{\overline{I}} \right) \right]^{-1} \cdot \overline{I}$$

In order to prepare a pre-reduced Fe_3O_4-Cu sample, Fe_2O_3-Cu (0.2g, Cu/Fe=0.01) was treated in 20 % H_2 in Ar (total flow rate 100 cm^3/min, ramping rate 5 K/min) at temperatures up to 533 K, where Fe_2O_3-Cu was reduced to Fe_3O_4-Cu in H_2 after the first step of reduction. The pre-reduced sample was then cooled down to 523 K in He (100 cm^3/min) before switching the flow to synthesis gas.

Table 1 Mass fragmentation matrix for the main products during the reduction and carburization of Fe-K-Cu oxides in mixture of H_2/CO at 250 ^oC

1. Mass Spectrum Deconvolution Matrix (November 17, 1999)

Mass	**H_2**	**CH_4**	**H_2O**	**CO**	**Ar**	**CO_2**
Intensity Response Factors	1.105	1.1572	1.3907	1.4463	1	1.89
(R.F. = $I_i/I_{Ar}*X_{Ar}/X_i$)						
2	**1**	0.01031	0.005	0.00205	0	0.011
16	0	**1**	0.02226	0.00618	0	0.11
18	0	0	**1**	0.00502	0	0.01675
28	0	0	0	**1**	0	0.125
40	0	0	0	0	**1**	0
44	0	0	0	0	0	**1**

2. Mass Fragmentation Pattern Matrix times Response Factors Array

	H_2	CH_4	H_2O	CO	Ar	CO_2
2	1.11E+00	1.19E-02	6.95E-03	2.96E-03	0.00E+00	2.08E-02
16	0.00E+00	1.16E+00	3.10E-02	8.94E-03	0.00E+00	2.08E-01
18	0.00E+00	0.00E+00	1.39E+00	7.26E-03	0.00E+00	3.17E-02
28	0.00E+00	0.00E+00	0.00E+00	1.45E+00	0.00E+00	2.36E-01
40	0.00E+00	0.00E+00	0.00E+00	0.00E+00	1.00E+00	0.00E+00
44	0.00E+00	0.00E+00	0.00E+00	0.00E+00	0.00E+00	1.89E+00

3. Inverted Response Matrix

	1	2	3	4	5	6
1	9.05E-01	-9.33E-03	-4.32E-03	-1.78E-03	0.00E+00	-8.63E-03
2	0.00E+00	8.64E-01	-1.92E-02	-5.24E-03	0.00E+00	-9.41E-02
3	0.00E+00	0.00E+00	7.19E-01	-3.61E-03	0.00E+00	-1.16E-02
4	0.00E+00	0.00E+00	0.00E+00	6.91E-01	0.00E+00	-8.64E-02
5	0.00E+00	0.00E+00	0.00E+00	0.00E+00	1.00E+00	0.00E+00
6	0.00E+00	0.00E+00	0.00E+00	0.00E+00	0.00E+00	5.29E-01

4. M*M-1

1.00	0.00	0.00	0.00	0.00	0.00
0.00	1.00	0.00	0.00	0.00	0.00
0.00	0.00	1.00	0.00	0.00	0.00
0.00	0.00	0.00	1.00	0.00	0.00
0.00	0.00	0.00	0.00	1.00	0.00
0.00	0.00	0.00	0.00	0.00	1.00

In order to prepare a pre-carburized Fe_xC-Cu samples, Fe_2O_3-Cu (0.2g, Cu/Fe=0.01) was pretreated in 20 % CO in Ar (total flow rate 100 cm^3/min, ramping rate 5 K/min) at temperatures up to 673 K. The ramping rate was kept low in order to terminate the reaction in a way that Fe_2O_3-Cu was reduced and carburized to Fe_xC-Cu in CO without the contamination by graphite deposits formed in Boudouard reactions favored at high temperatures. The pre-carburized sample was then cooled down to 523 K in He (100 cm^3/min) before switching the flow to synthesis gas.

3.3. In-situ X-ray Absorption (XAS) Measurements of Initial Phase Evolution in FTS

In-situ X-ray absorption near-edge (XANES) and extended X-ray absorption fine structure (EXAFS) measurements were continued during this reporting period at the Stanford Synchrotron Radiation Laboratory (SSRL). The emphasis was on the *in-situ* Fe K-edge analyses of the effects of K and Cu on the initial reduction and carburization behavior of Fe oxides in synthesis gas. Fe K-edge spectra of Fe-K-Cu oxides were measured during reduction and carburization in synthesis gas using an *in-situ* XAS cell designed by Barton *et al.* (18). The cell consists of a 0.8 mm external diameter quartz tube with 0.1 mm wall thickness connected to a gas manifold. A 1.2×0.2 mm X-ray beam passed through the heated zone of the capillary cell during reactions (Appendix 3.1). Typically, 8 mg of catalyst (diluted to ~10 wt% Fe using graphite) was loaded into the cell and synthesis gas with a H_2/CO ratio of 2 was used at a gas hourly space velocity of 6000 and 523 K. This design also accommodates rapid cooling of the quartz cell to room temperature by simply sliding the heated zone back from the cell.

3.4. Switch Transient of Fe_2O_3 in Synthesis Gas

Figure 1.1 shows the isothermal transients measured at 523 K during reduction and carburization and subsequent FTS of pure Fe_2O_3 in synthesis gas (H_2/CO=2). In addition to H_2O and CO_2, hydrocarbons formed after an initial induction period. Here, we use CH_4 formation rate as a useful measure of the relative rates of FTS, because of the difficulty in distinguishing individual higher hydrocarbons using their fragmentation patters within a complex composite mass spectrum. During the initial 140 s after exposure to H_2/CO, only Fe_2O_3 reduction occurred, as indicated by the predominant evolution of the H_2O and CO_2 reduction products, without the concurrent formation of CH_4 or other hydrocarbons. The extent of initial reduction (dashed area) shows that about 7 % of the O-atoms (ca 10 monolayers) in Fe_2O_3 are removed by H_2 (O/Fe=0.01) forming H_2O or by CO (O/Fe=0.09) to form CO_2. It appears that partially reduced Fe_2O_3 (i.e., O-deficient Fe_2O_{3-x} (x=0-0.2)) formed initially is not active for FTS and that FTS reactions occur only after a distinct structural phase change to form Fe_3O_4 occurs. CH_4 formation rates start to increase after about 140 s in H_2/CO and reach steady-state after 240 s.

In-situ X-ray absorption spectroscopy measurements (Figure 1.2) during the initial FTS reaction show that neither Fe_3O_4 nor Fe carbide is formed within the induction period. After the induction period, Fe_3O_4 and Fe carbides formed concurrently and the extent of carburization increases with time on stream. This suggests that O-deficient Fe_2O_3 goes through a structural change to Fe_3O_4 only when O vacancies accumulate to a certain

concentration, which leads to the local nucleation of the new Fe_3O_4 phase; the conversion of the surface layers of Fe_3O_4 to Fe carbide then proceeds very rapidly. Fe_3O_4 oxides continue to carburize with time, but the formation rate of CH_4 reaches a steady-state value. This indicates that only near-surface carbide layers are required to form FTS active sites; the catalytic activity of Fe carbides is not influenced by the existence of Fe oxide cores within the particles or by its progressive carburization to Fe_xC.

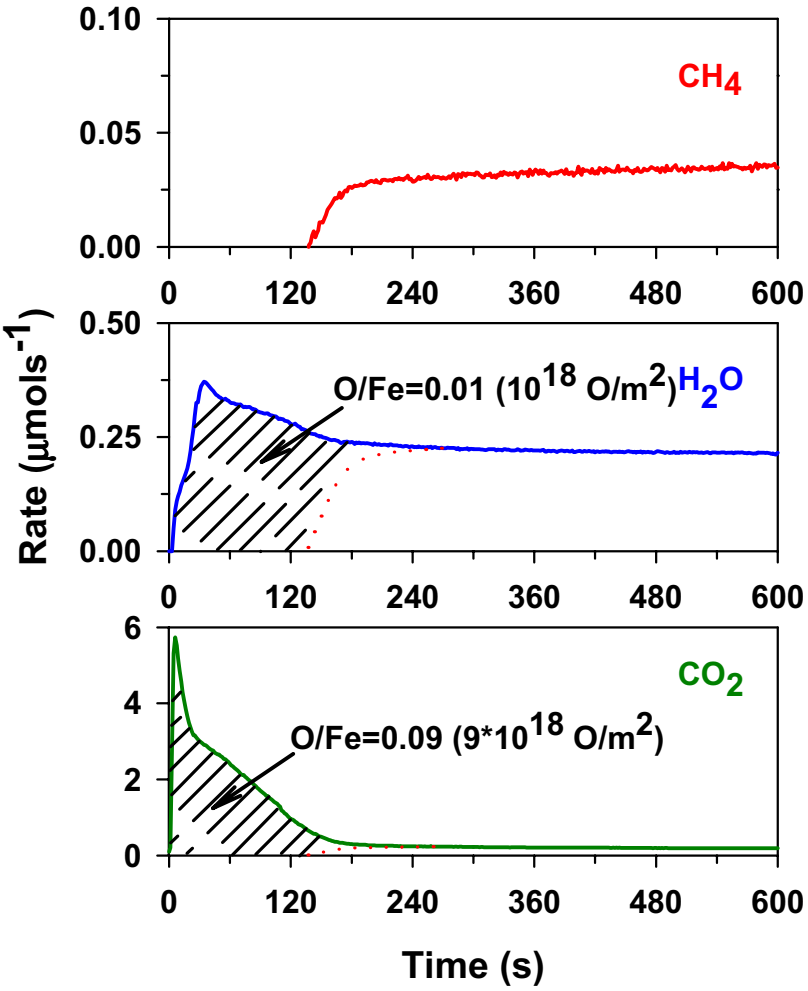

Figure 1.1 Isothermal product transient of Fe_2O_3 (0.2g) in synthesis gas (H_2/CO=2, 60 % synthesis gas in Ar, total flow rate 100 cm^3/min) at 523 K.

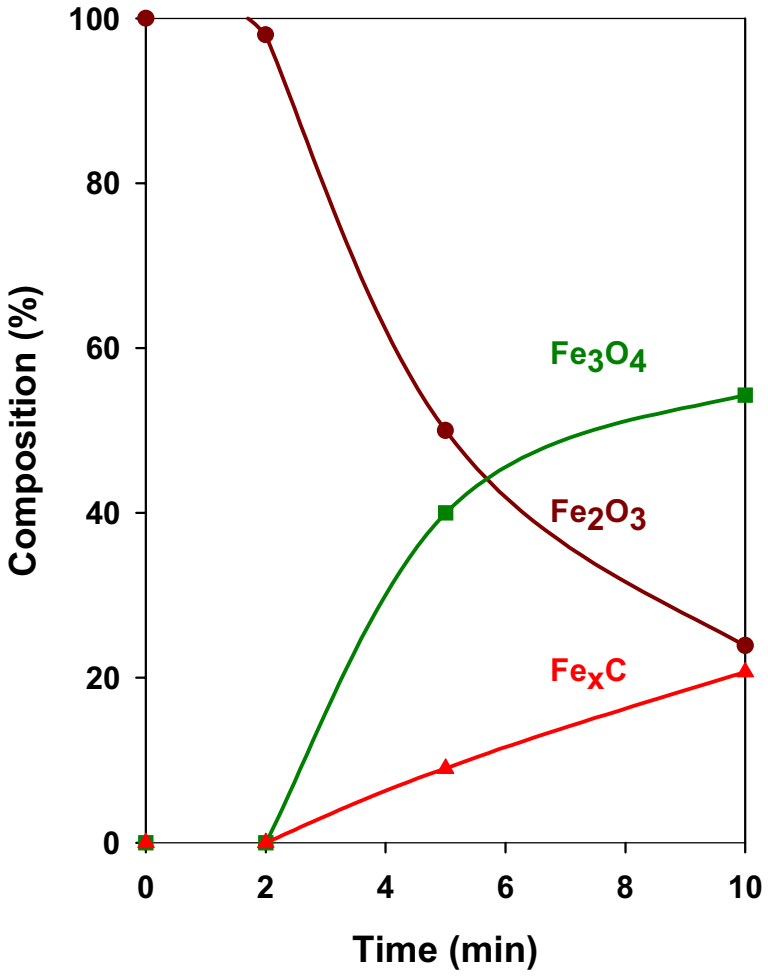

Figure 1.2 *In-situ* Fe K-edge linear combination XANES fit of Fe_2O_3 (8 mg sample (10 wt% Fe)) in synthesis gas (H_2/CO=2, GHSV= 6000) at 523 K.

The Fe K-edge linear combination XANES fit of Fe_2O_3 can be used in order to monitor the structural evolution during 10 h in H_2/CO mixture (Table 1.2). The extent of reduction/carburization increased with time on stream at 523 K and the content of Fe carbides reaches a constant value (~30%) after ~4 h reaction. This indicates that the diffusion rates of oxygen and carbon are retarded after the initial formation of Fe carbides layers near the surface of Fe_3O_4 crystallites. Higher temperatures (543 K) increases the diffusion rates and increased the extent of carburization to 45%.

Table 1.2 Fe K-edge linear combination XANES fit showing the structural evolution of Fe_2O_3 during FTS (1 mg coprecipitated Fe_2O_3, 52 m^2/g, H_2/CO=2, 6000 GHSV)

Temperature (K)	Time (h)	Fe_2O_3 (%)	Fe_3O_4 (%)	Fe_xC (%)
523	0.5	29	48	24
	1	26	45	28
	2	3	66	31
	4	1	68	31
	10	-	69	31
543	2	-	58	42
	4	-	54	45

Figure 1.4 illustrates the effects of these structural transformations on FTS rates. The concentration of Fe_2O_3 decreased significantly while those of Fe_3O_4 and Fe carbides increased with time on stream until they all reached a steady-state value. Following the similar evolution trend as Fe carbides, FTS rates increased and approached their steady-state values. These results confirm that FTS rates are only related to the formation of surface Fe carbides.

In view of the measured FTS rate transients and X-ray absorption data, we present a contracting sphere model in order to describe the reduction and carburization of Fe_2O_3 in synthesis gas (Figure 1.5). In this model, surface oxygen ions in Fe_2O_3 are removed from the lattice by reduction, leaving behind O-deficient Fe_2O_3. When the concentration of vacancies reaches a critical value, the structure rearranges to Fe_3O_4 in the near surface regions with Fe_2O_3 core still inside. The fresh Fe_3O_4 surface is readily reduced and carburized to Fe carbides, in which FTS reactions are initiated. At this point, the particle consists of three local regions with Fe compounds of distinct composition and structure throughout the sphere: Fe_2O_3, Fe_3O_4 and Fe_xC. As the reduction and carburization proceed, the boundary of innermost core of Fe_2O_3 contracts and eventually disappears, leaving an Fe_3O_4 core covered by carbides. At the same time, the outward oxygen diffusion rates and inward carbon diffusion rates progressively decreases as additional Fe carbide layers form. The diffusion rates ultimately become so slow after 4 h reaction in H_2/CO that the composition of particles reaches a steady-state value and it does not change during an additional 6 h on stream.

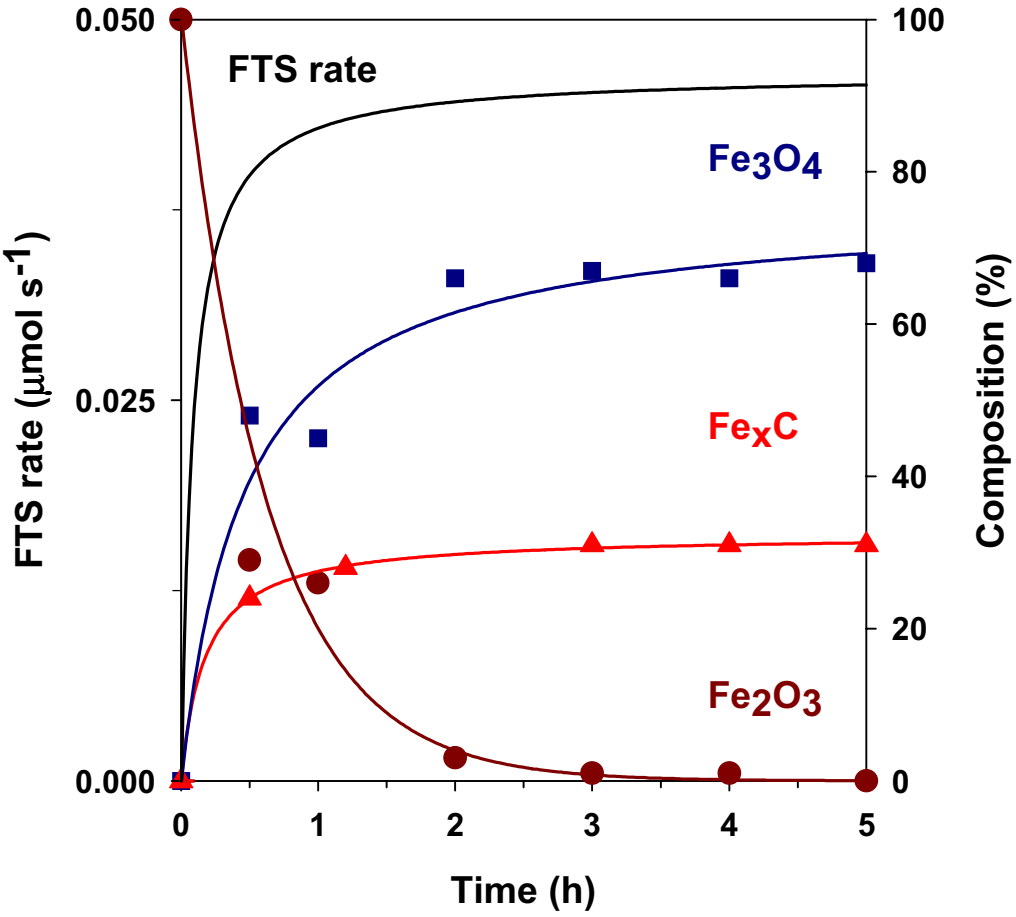

Figure 1.3 FTS rates (0.2 g Fe_2O_3, $H_2/CO=2$, 60 % synthesis gas in Ar, total flow rate 100 cm^3/min) and *in-situ* XAS phase compositions (1 mg Fe_2O_3) as a function of time in synthesis gas ($H_2/CO=2$, GHSV= 6000) at 523 K.

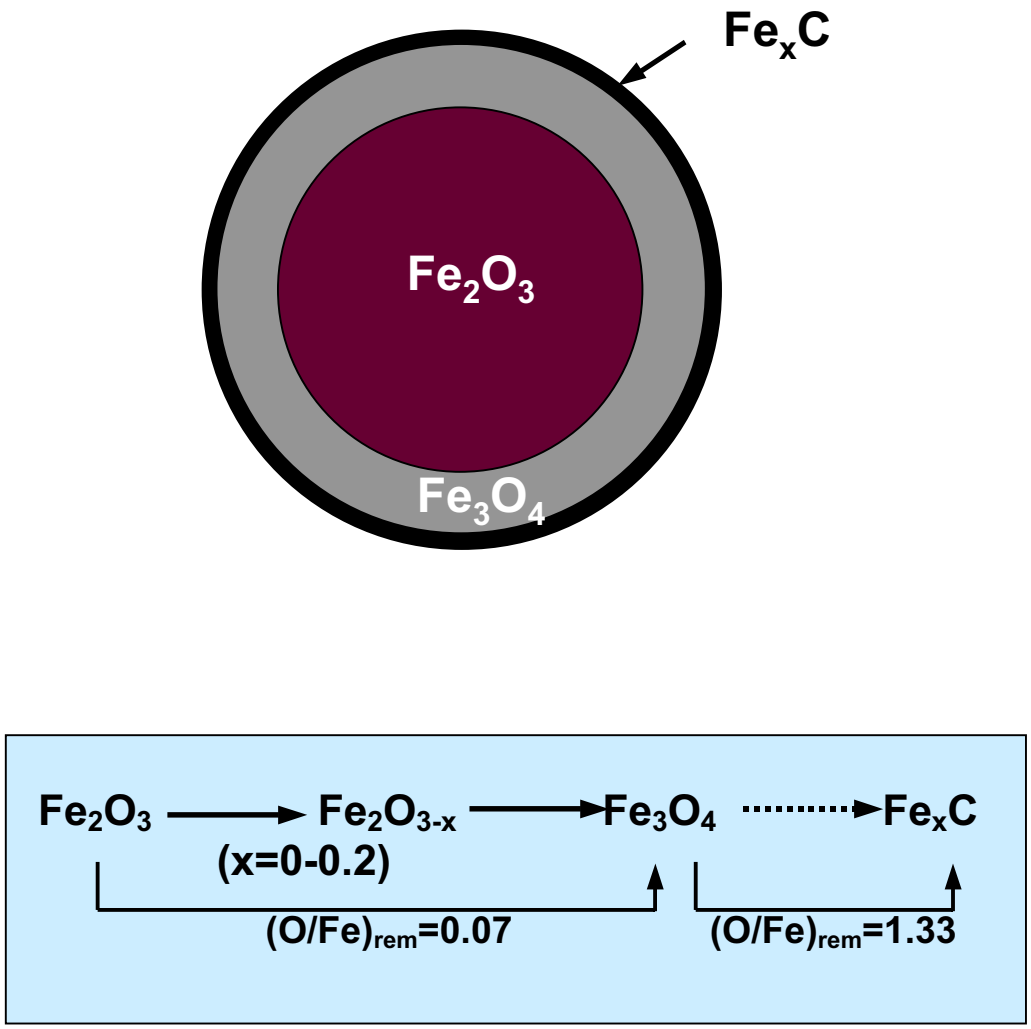

Figure 1.4 Contracting sphere model of Fe_2O_3 in synthesis gas

3.5. Switch Transient of Fe_2O_3-Cu in Synthesis Gas: Effect of Cu

Figure 1.5 shows isothermal transient for the reduction and carburization of Fe-Cu oxide (Cu/Fe=0.01) in synthesis gas at 523 K. Sharp H_2O and CO_2 peaks followed by a broader peak during the first 2 min are observed after exposure to synthesis gas. CuO reduced in H_2 at 453 K; the amount of H_2O and CO_2 formed under initial peaks corresponds to that for the reduction of CuO to Cu. Therefore, the first sharp H_2O and CO_2 peaks can be ascribed to the reduction of CuO to Cu. Compared with pure Fe_2O_3, a significant amount of H_2O forms during the initial induction period on Cu-Fe oxide. Cu apparently increases the rate of Fe_2O_3 reduction to Fe_3O_4 by dissociating H_2. The extent of initial reduction shows that about 7 % of the O-atoms (~ 10 monolayers in Fe_2O_3) are removed by H_2 (O/Fe=0.07) forming H_2O or by CO (O/Fe=0.03) yielding CO_2. Although the more O-atoms are removed from Fe_2O_3-Cu by H_2 than by CO in comparison with the Cu-free sample, the total amount of O-atoms removed during initial reduction (O/Fe=0.1) is very similar to those removed from pure Fe_2O_3. This suggests that the reduction and carburization of Fe_2O_3-Cu follow the same mechanism as that of Fe_2O_3. Cu simply increases the rate of oxygen removal by allowing the more efficient use of H_2. Methane, which starts to form after about 1 min, reaches a steady-state formation rate slightly higher rate than measured on Fe_2O_3. This indicates that Cu not only increases reduction and carburization rates but it also increases FTS rates by dissociating H_2. This may reflect a higher H_2 dissociation rate during FTS, but the similar selectivities obtained on Fe-Cu and Cu-free samples (see Figure 1.17) is not consistent with this proposal. Higher dissociation rates would lead to smaller and more paraffinic FTS products. Instead, it appears that the presence of Cu increases the nucleation rate of Fe_3O_4 or Fe_xC crystallites, a process that would lead to the formation of smaller crystallites with higher active surface areas anf to higher FTS rates with minimal changes in selectivity.

In-situ X-ray absorption spectroscopy XANES fit of Fe_2O_3-Cu in a mixture of H_2/CO at 523 K (Figure 1.6) showed that Fe_2O_3-Cu goes through similar structural evolution as Fe_2O_3. In other words, Fe_2O_3 initially disappeared during the FTS induction period and Fe_3O_4 and Fe carbides formed concurrently and the extent of reduction and carburization increased with time on stream. However, Fe_3O_4 and Fe_xC first appeared about 1 minute earlier than on the Cu-free Fe_2O_3 sample and the concentrations of Fe_3O_4 and Fe_xC are higher in Fe_2O_3-Cu than in Fe_2O_3 at the same period of exposure time. These results are consistent with the switch transient studies, which show that Cu increases reduction and carburization rates and consequently shortens the initial induction period. Figure 1.7 shows the reduction and carburization model of Fe_2O_3-Cu in synthesis gas, which resembles the contracting sphere model proposed for pure Fe_2O_3. Cu dissociates H_2 and thus facilitates the reduction process required for carburization by CO to start, increasing the nucleation rate for Fe_3O_4 and Fe_XC, their ultimate surface areas, and the FTS rates.

3.6. Switch Transient of Fe_xC-Cu and Fe_3O_4-Cu in Synthesis Gas

The results described in the previous sections appear to show that Fe carbides provide the active species for FTS reactions. Therefore, our next step was to obtain additional evidence by examining the reaction transients using a Fe_2O_3-Cu sample pre-carburized in CO before exposure to synthesis gas. Fe_2O_3-Cu was pre-carburized in CO at a ramping rate of 5 K/min up to a final temperature of 673 K. Both the ramping rate (5 K/min) and the temperature (up to 673 K) were chosen in order to minimize carbon deposition via Boudouard reactions favored at higher temperatures. As shown in Figure 1.8, the reaction proceeds via sequential reduction and carburization steps. Fe_2O_3 is first reduced to Fe_3O_4 and then reduced/carburized to form Fe carbide. X-ray diffraction proved that the phase composition after the reaction was a mixture of $Fe_{2.5}C$ and Fe_3C (hereafter abbreviated as Fe_xC).

Figure 1.9 shows the isothermal transient of the reduction and carburization of pre-carburized Fe-Cu oxide (Cu/Fe=0.01) in synthesis gas at 523 K. No induction period for CH_4 formation was detected. The CH_4 formation immediately reached a constant rate upon exposure to synthesis gas, and this value was similar to that observed on Fe_2O_3-Cu sample activated in synthesis after achieving steady state. The same immediate response was observed for the H_2O and CO_2 products of FTS reactions. The similar CH_4 formation rates on Fe_xC-Cu as on Fe_2O_3-Cu at steady state indicates that FTS rates are not influenced by the presence of an Fe oxide core. This observation confirms the conclusion that Fe carbides are the active phase for FTS reaction; the catalytic properties of Fe carbides do not depend on the presence of an Fe oxide core. It appears that there are very small amounts of oxygen removed from Fe carbide at the initial reduction period. These are likely to arise from trace oxygen impurities in the He carrier gas used to flush the CO reactants used for the pre-carburization step. In view of this, we cannot the residual presence of an Fe oxycarbide phases, FeC_xO_y, but neither this phase nor Fe_2O_3 or O-deficient Fe_2O_{3-x} are the active phases for FTS reactions.

We also measured reaction transients of Fe_3O_4 in synthesis gas in order to examine the possibility of Fe_3O_4 being the active phases. Fe_2O_3-Cu (Cu/Fe=0.01) was pre-reduced in H_2 at temperatures up to 533 K in order to Fe_3O_4-Cu powders with high phase purity (measured by X-ray diffraction). Figure 1.10 shows that the isothermal transients for the reduction and carburization of pre-reduced Fe_3O_4-Cu in synthesis gas at 523 K. Similar to Fe_xC-Cu, the CH_4 formation rates reached a constant value almost immediately upon exposure to synthesis gas. Significant excess amounts of CO_2 and H_2O formed after initial exposure to synthesis gas, suggesting the progressive reduction and carburization of the starting Fe_3O_4-Cu powders. These observations indicate that Fe_3O_4 carburizes rapidly in contact with synthesis gas at 523 K, and that near surface regions reach their active carbide state within the typical time of an FTS turnover, leading to the absence of an initial induction period for FTS reaction rates. These data confirm that FTS rates depend only on the composition of the near surface layers and that the carburization of Fe_3O_4 occurs in the time scale of the catalytic reaction. These features of the solid state and catalytic chemistry has led to the earlier contradictory conclusions about the nature of oxides and carbides of Fe as the active phase for the FTS reaction.

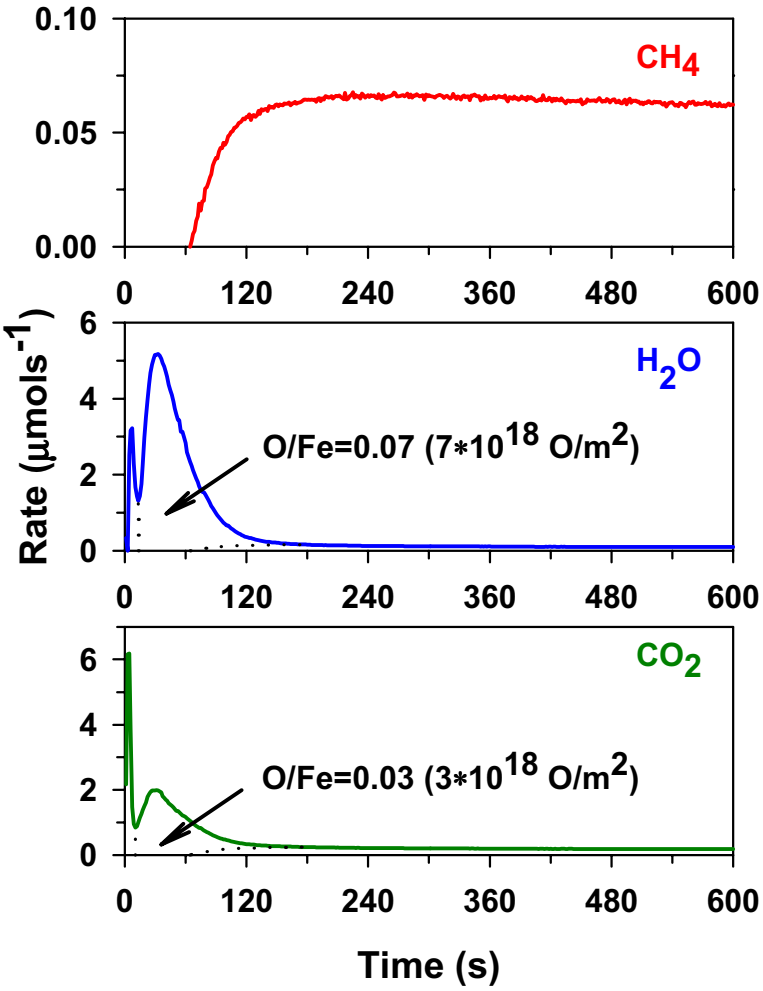

Figure 1.5 Isothermal product transient of Fe_2O_3-Cu (0.2 g, Cu/Fe=0.01) in synthesis gas (H_2/CO=2, 60 % synthesis gas in Ar, total flow rate 100 cm^3/min) at 523 K.

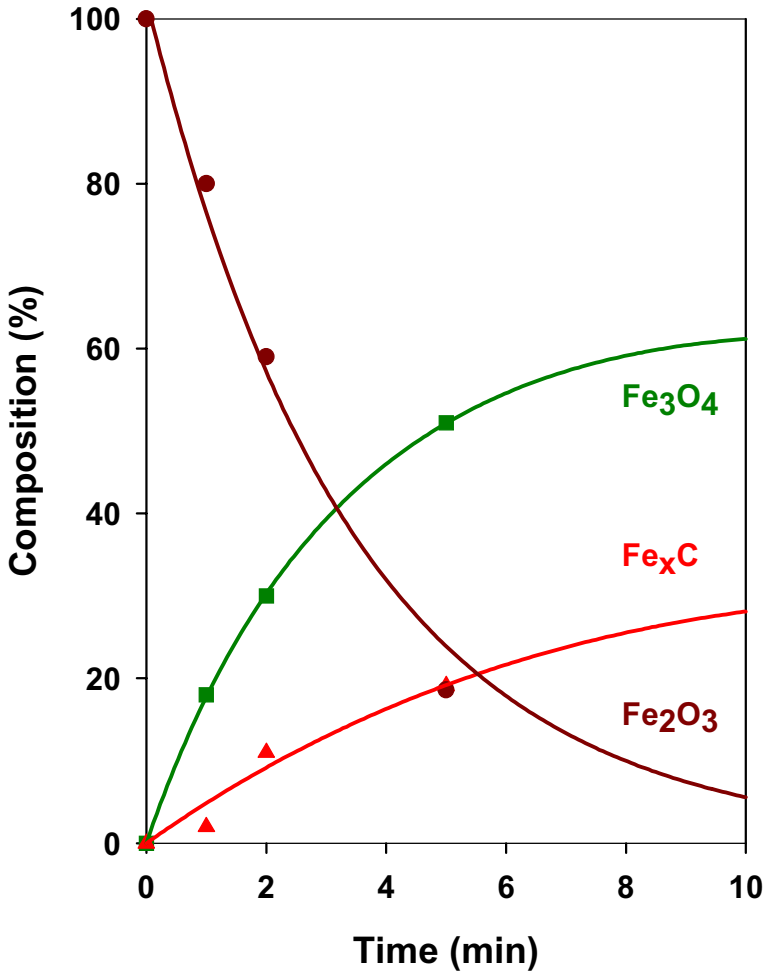

Figure 1.6 *In-situ* Fe K-edge linear combination XANES fit of Fe_2O_3-Cu (1 mg) in synthesis gas (H_2/CO=2, GHSV= 6000) at 523 K.

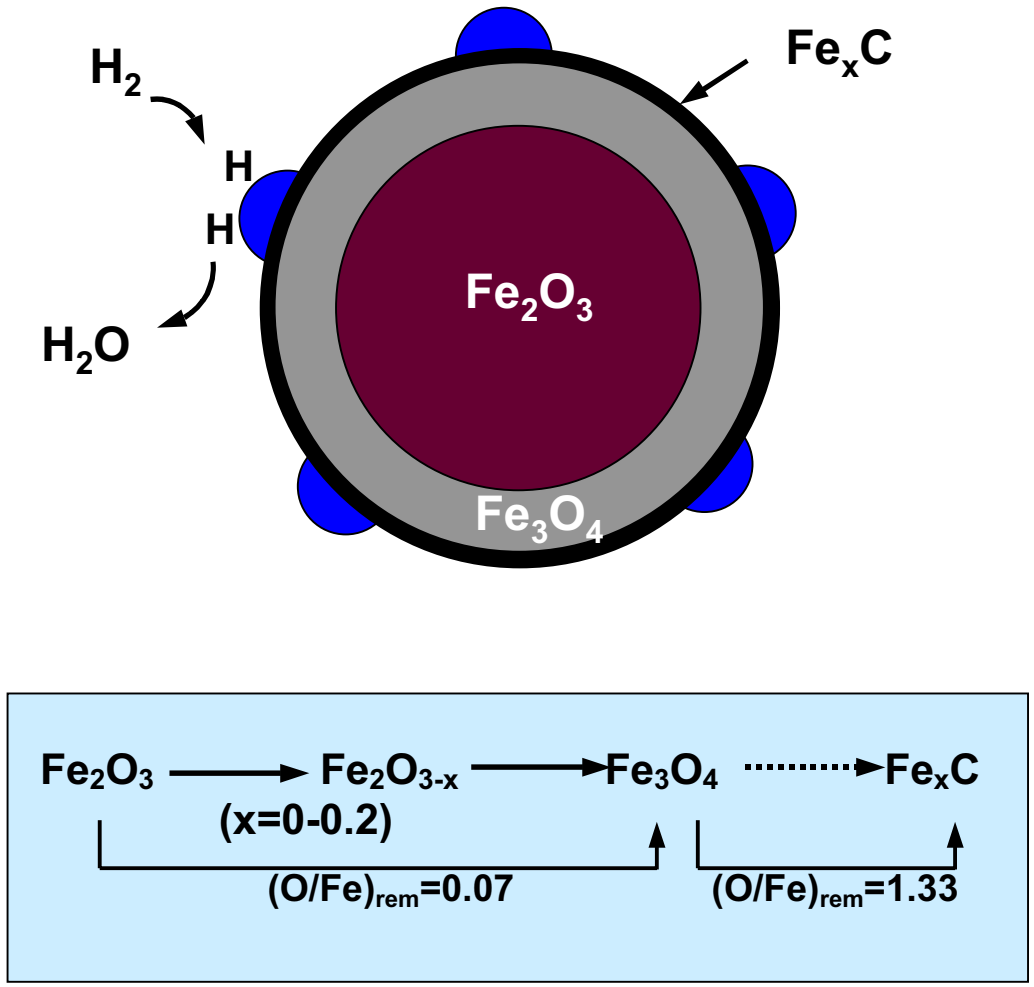

Figure 1.7 Contracting sphere model of Fe_2O_3-Cu in synthesis gas

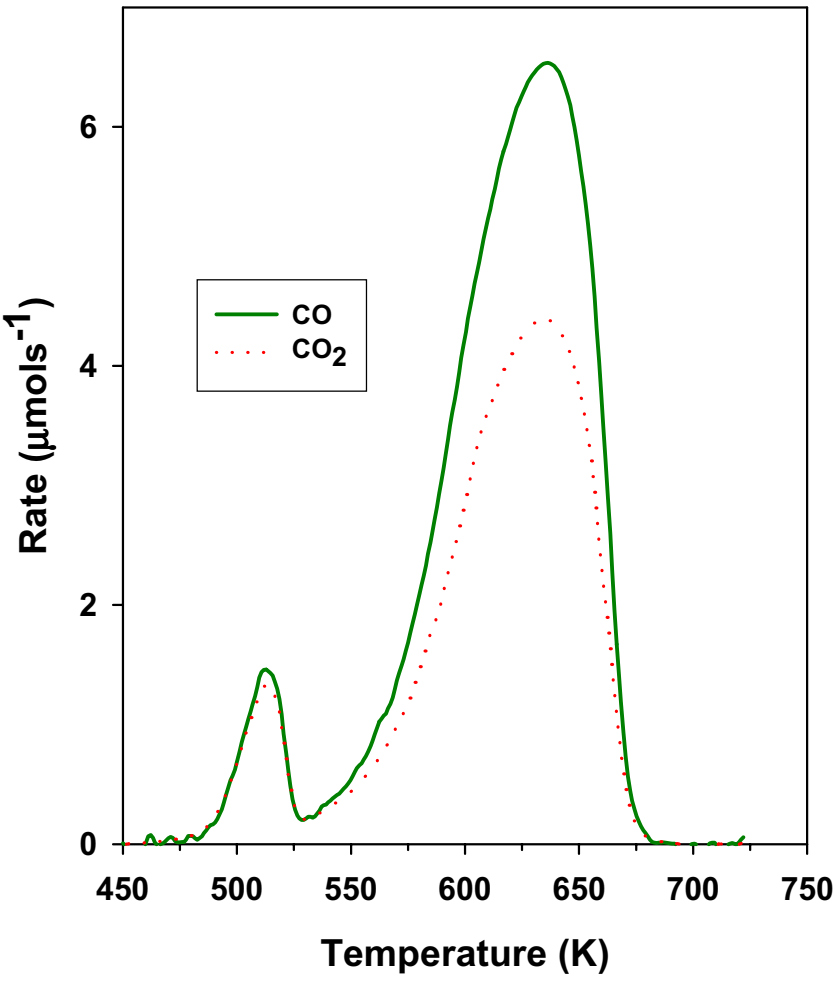

Figure 1.8 Temperature-programmed carburization of Fe_2O_3-Cu in CO (0.2 g, 5 K/min ramping rate, 20% CO in Ar, 100 cm^3/min flow rate) at temperatures up to 673 K.

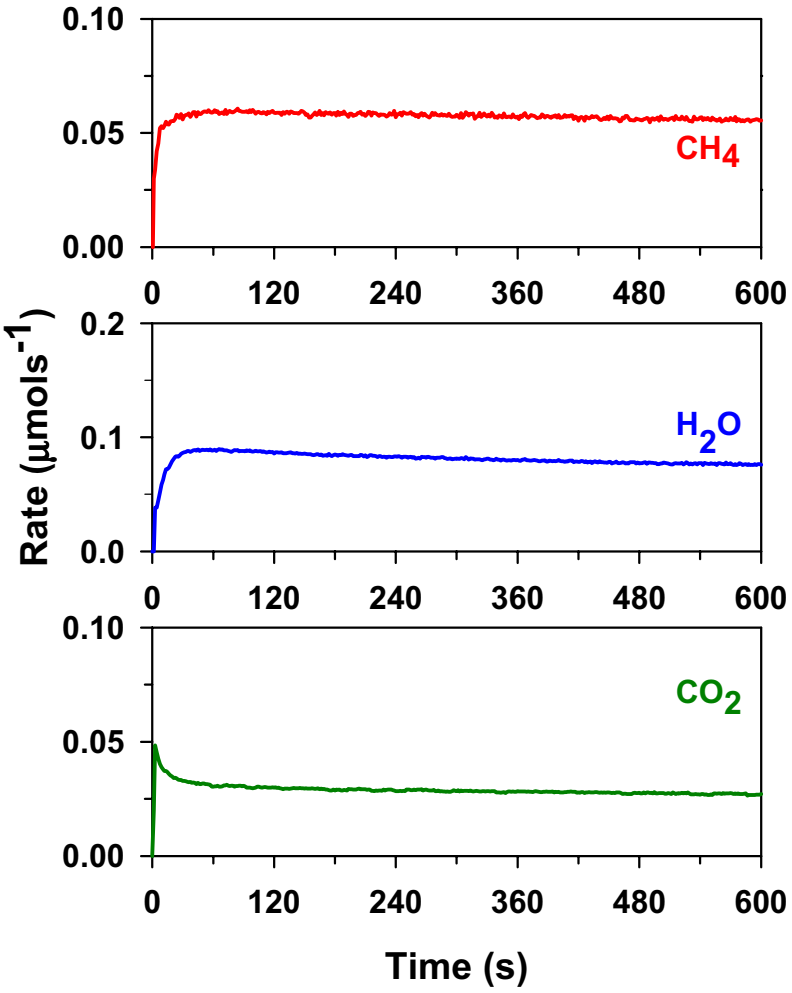

Figure 1.9 Isothermal product transient of pre-carburized Fe_xC-Cu (0.2 g, Cu/Fe=0.01) in synthesis gas (H_2/CO=2, 60 % synthesis gas in Ar, total flow rate 100 cm^3/min) at 523 K.

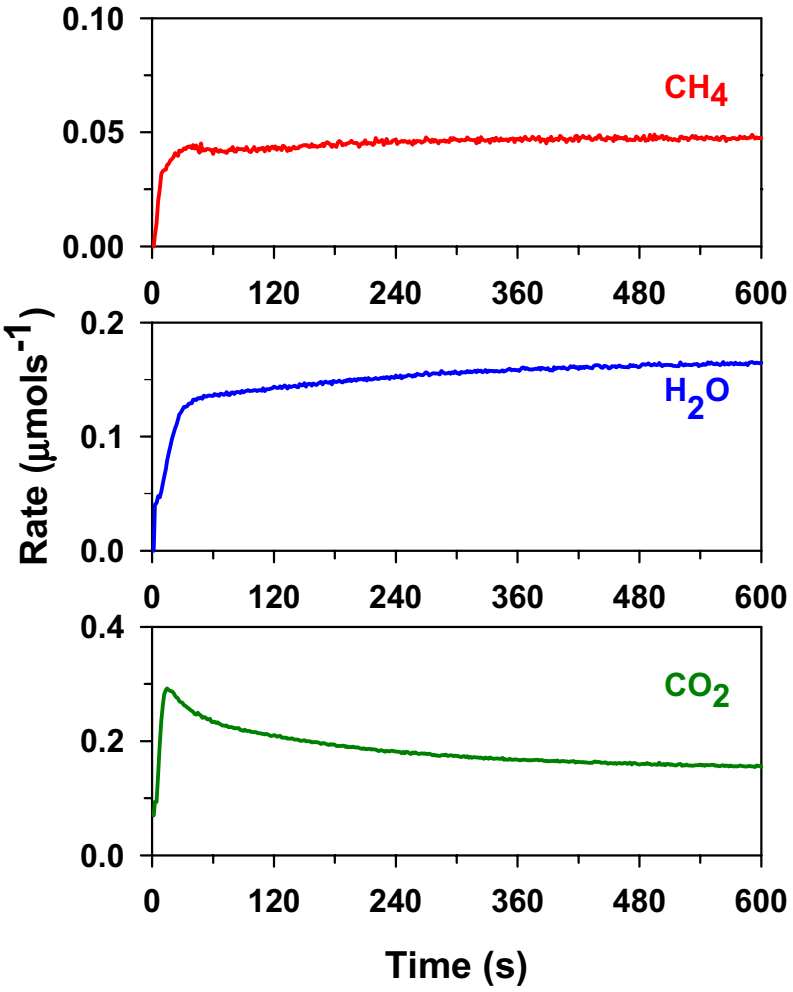

Figure 1.10 Isothermal product transient of pre-reduced Fe_3O_4-Cu (0.2 g, Cu/Fe=0.01) in synthesis gas (H_2/CO=2, 60 % synthesis gas in Ar, total flow rate 100 cm^3/min) at 523 K.

3.7. Switch Transient of Fe_2O_3-K in Synthesis Gas: Effect of K

Figure 1.11 shows isothermal transients for reduction and carburization of Fe_2O_3-K (K/Fe=0.02) in synthesis gas at 523 K. Compared with Fe_2O_3, the reduction and carburization of K-promoted Fe_2O_3 showed a more complex evolution of structure, composition, and catalytic behavior. After a very short induction period, CH_4 formation rates increased significantly and then decreased gradually with time on stream. H_2O evolution shows a sharp peak followed by a broader peak within the initial ten minutes of exposure to synthesis gas. There is also a very sharp initial peak of CO_2 as the sample is exposed to synthesis gas. X-Ray absorption measurements confirmed the gradual reduction of Fe_2O_3-K and the concurrent formation of Fe_3O_4 and Fe_xC within the first two minutes after exposure to synthesis gas (Figure 1.12). However, the extent of reduction and carburization of Fe_2O_3-K is smaller than for Fe_2O_3 after this induction period (2 min). This indicates that K assists the initial formation of Fe carbides, but not the further reduction and carburization of the residual oxide core in the catalyst.

Based on previous studies on reduction behaviors of transitional metal oxides (19), a nucleation-growth model would be able to explain the complex effects of K on the reduction and carburization of Fe_2O_3 in synthesis gas (Figure 1.13). Because of the electron donation effect of K on Fe, CO is preferentially activated near the interface between Fe_2O_3 and K_2CO_3, leading to the local reduction of Fe_2O_3 near this interface. This leads to the sharp CO_2 evolution peak observed initially upon exposure to H_2-CO and to the subsequent carburization of the Fe_3O_4 to form the active Fe_xC and to start the formation of FTS reaction products. As Fe_xC form, another interface forms between Fe_xC and Fe_2O_3. CO dissociation occur preferentially along this interface and the FTS reaction rate increases with increasing time on stream, as indicated by the gradual initial increase in the rate of formation CH_4, H_2O and CO_2 FTS products. As reduction and carburization proceed further, carbide domains increase and carbide-oxide and carbide-K_2CO_3 interfacial regions begin to disappear as carbide domains overlap and large carbide regions cover most of the surface. Consequently, CH_4 formation rates go through a maximum and then decrease with the loss of interfacial contacts. K species in the form of K_2CO_3 initiate the reduction and carburization of Fe_2O_3 upon exposure to synthesis gas but the initial reduction rate is lower than for Fe_2O_3. This observation is consistent with our previous studies of the reactions of Fe_2O_3 with CO, which showed that reduction of Fe_2O_3 to Fe_3O_4 was inhibited by K addition (23). As Fe carbide forms, however, it increases the H_2 and CO dissociation rates, and thus increases the rate of reduction of Fe oxides, as indicated by the broad peak of H_2O and CO_2. As most of the O atoms are removed from the Fe oxides, both H_2O and CO_2 formation rates decrease and reach a steady state corresponding to their rate of formation as the oxygen-containing end product of FTS reactions.

3.8. Switch Transient of Fe_2O_3-Cu-K in Synthesis Gas: Synergetic Effect of Cu and K

Figure 1.14 shows isothermal transients for the reduction and carburization of Fe-K-Cu oxides (K/Fe=0.02, Cu/Fe=0.01) in synthesis gas at 523 K. The transient evolution of H_2O and CO_2 on Fe-K-Cu oxides were similar to those for Fe-Cu oxides, except that CO was more significantly involved in the reduction of Fe_2O_3 during the induction period. The CH_4 formation transient resembles that for Fe_2O_3-K. The addition of K to Fe-Cu oxides led to steady-state CH_4 formation rates about three times higher than on Fe-Cu oxides after 600 s reaction. The higher CO reduction and FTS rates obtained upon addition of K to Fe-Cu oxides apparently reflect the effect of K in promoting CO dissociation rates on Fe carbides, consistent with previous proposals that alkali increase CO adsorption energies and dissociative chemisorption rates (20, 21). Since Cu dissociates H_2 and K assists CO dissociation on Fe, an appropriate combination of Cu and K may provide a proper surface hydrogen and carbon ratio that leads to a maximum -CH_2- monomer and thus, gives the highest FTS rates.

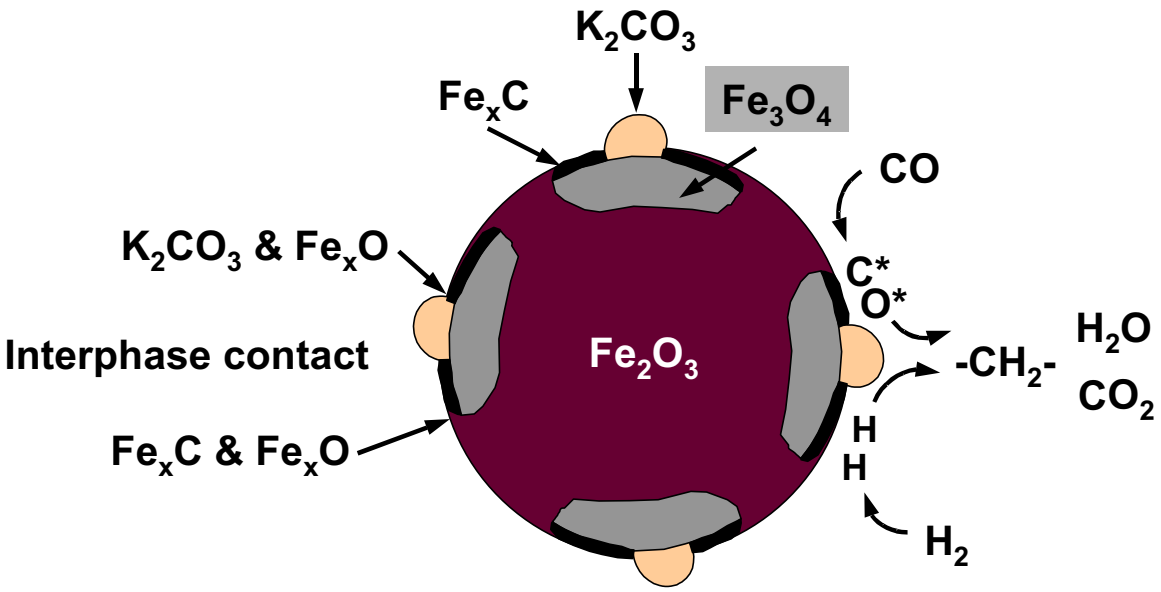

Figure 1.13 Nucleation model of Fe_2O_3-K in synthesis gas

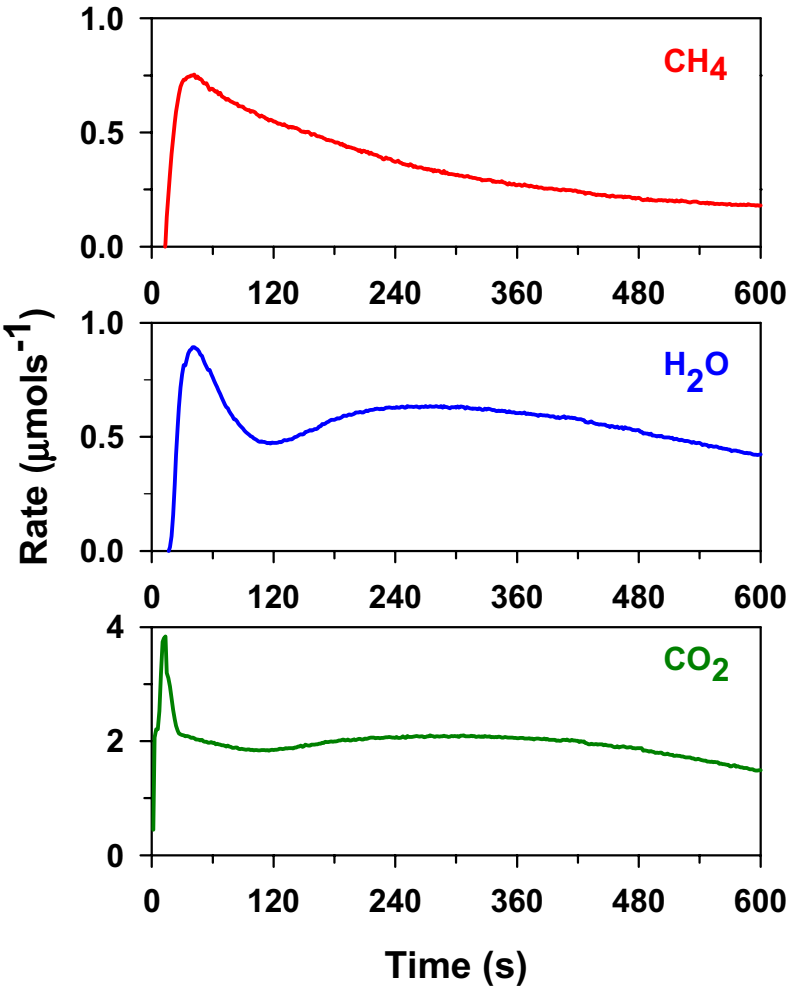

Figure 1.11 Isothermal product transient Fe_2O_3-K (0.2g, K/Fe=0.02) in synthesis gas (H_2/CO=2, 60 % synthesis gas in Ar, total flow rate 100 cm^3/min) at 523 K.

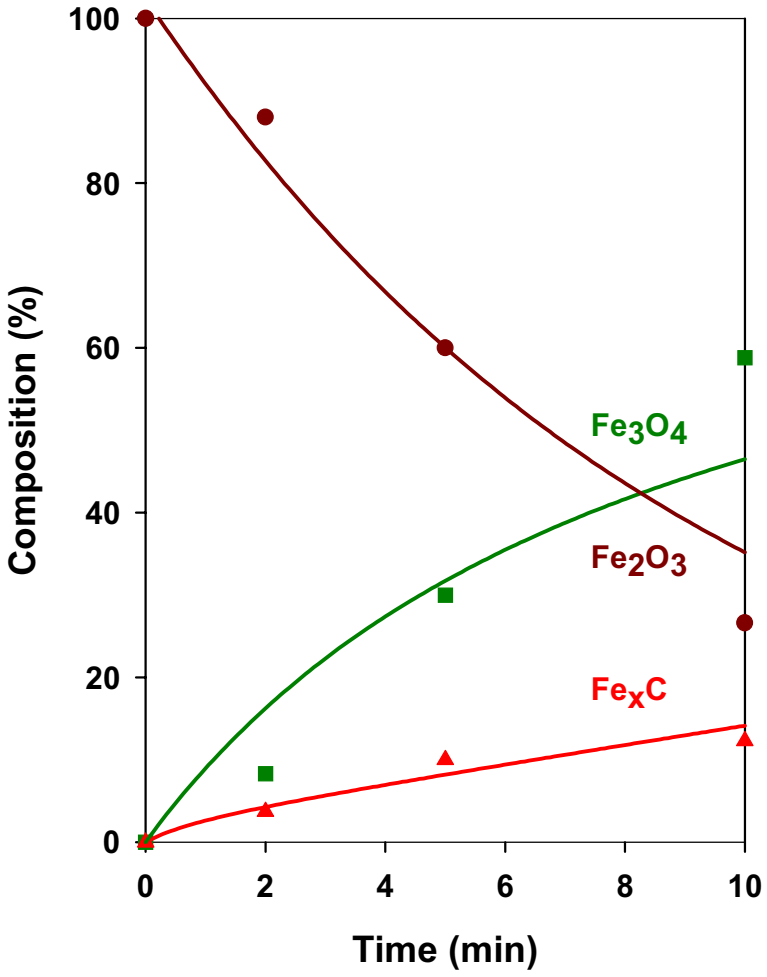

Figure 1.12 *In-situ* Fe K-edge linear combination XANES fit of Fe_2O_3-K (1 mg) in synthesis gas (H_2/CO=2, GHSV= 6000) at 523 K.

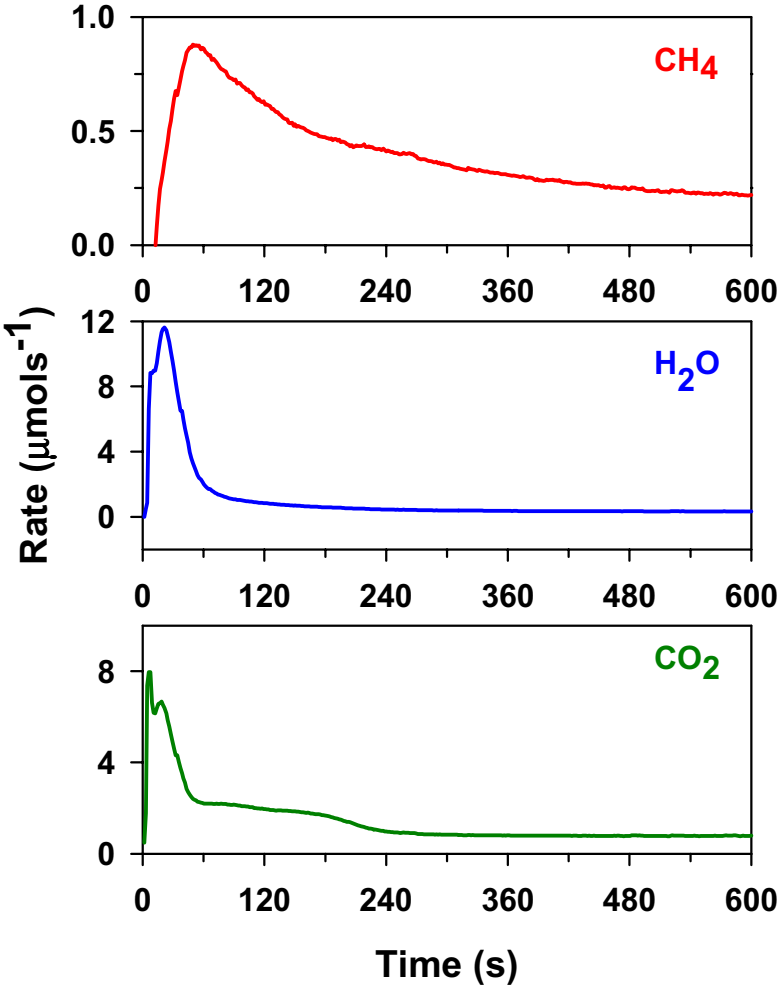

Figure 1.14 Isothermal product transient of Fe_2O_3-Cu-K (0.2 g, Cu/Fe=0.01, K/Fe=0.02) in synthesis gas (H_2/CO=2, 60 % synthesis gas in Ar, total flow rate 100 cm^3/min) at 523 K.

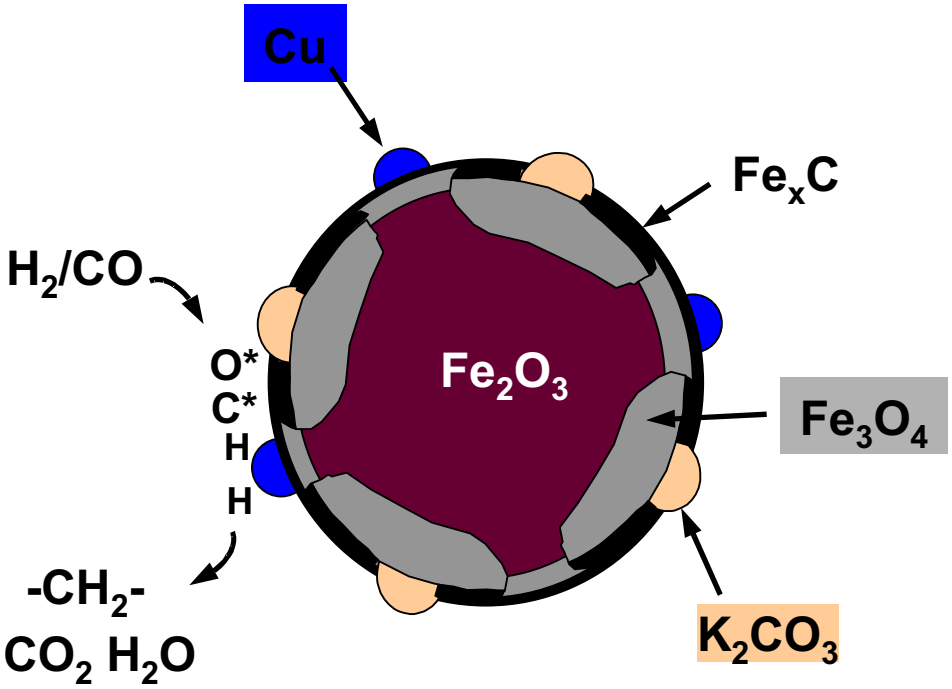

Figure 1.15 A combination of contracting sphere and nucleation model of Fe_2O_3-Cu-K in synthesis gas.

3.9 Effects of K and Cu Effects on the Catalytic Properties of Fe_2O_3-K-Cu

In this section, we examine the effects of K and Cu on FTS reaction rates at more realistic conditions and with a more complete analysis of the product distribution than in the isothermal transient studies described in the previous sections.

Fig. 1.16 shows the CH_x and CO_2 formation rate, C_{5+} selectivity and propene/propane ratio as a function of CO conversion on Fe-Cu catalysts (0.4 g, Cu/Fe=0.01) with varying K loading at 235 ^oC and 21.4 atm using synthesis gas reactants (H_2/CO=2). Both hydrocarbon and CO_2 formation rates were increased markedly upon K addition, indicating that K increases FTS and water-gas shift reaction rates. K also increased the selectivity to C_{5+} and the FTS chain growth probability. The effect of K on chain growth is very strong and the C_{5+} selectivity increased more than 30% after K addition. The promotion effects of K on hydrocarbon and CO_2 formation rates as well as on chain growth probability are in agreement with the results obtained from our switch transient studies showing that K increases CO dissociation rates and decreases CO binding energies because of its electron donation effects. The enhanced dissociation of CO increases surface carbon concentration, which favors the formation of monomer CH_2 and CO_2, and thus increases FTS rates and chain growth probability as well as water-gas shift reaction rates. In addition, we use the propene/propane ratio as a measure of secondary olefin hydrogenation activity and of hydrogen availability on the catalyst surface. The reaction results show that these ratios are almost independent of CO conversion on K-promoted catalysts, suggesting that secondary hydrogenation reactions of propene do not take place. In contrast, propene/propane ratio decreases with increasing CO conversion on the K-free catalyst, indicative of the presence of secondary hydrogenation of propene. This result is consistent with our previous studies (21) showing that K inhibits the reduction of Fe oxides in H_2 by decreasing H_2 chemisorption. Low hydrogen surface concentration will reduce the probability of chain termination to paraffins and increase the probability of chain termination by desorption of olefins since chain growth can terminate either by β-hydrogen abstraction to form α-olefin or by H-addition to form paraffins. Therefore, the effect of K is to increase FTS rate by increasing CO dissociation. It also acts to modify surface carbon and hydrogen ratio, through which it increases the selectivities to higher molecular weight and olefinic products**.**

Figure 1.17 shows hydrocarbon and CO_2 formation rates, C_{5+} selectivity, and propene/propane ratio as a function of CO conversion on Fe-K catalysts (0.4 g, K/Fe=0.02) with varying Cu loading at 235 ^oC and 21.4 atm in synthesis gas (H_2/CO=2). In the same manner as K, Cu increased hydrocarbon and CO_2 formation rates, indicating that Cu increases the activity of the catalyst for the FTS and water-gas shift reactions. Our TPSR results of Fe_2O_3-Cu in CO showed that Cu decreased the temperature required for reduction and carburization by increasing CO chemisorption (23). Our switch transient studies showed that Cu not only increased the reduction and carburization but also led to higher CH_4 formation rates. These results all suggest that Cu increases FTS rates and water-gas shift reaction rates by increasing CO chemisorption and H_2 dissociation on Fe. On the other hand, the effect of Cu on the selectivity to C_{5+} and on

propene/propane ratio was weaker than that of K because the effect of Cu on the surface carbon concentration is weaker than that of K.

4. Fischer-Tropsch synthesis on Fe-based catalysts in a fixed bed reactor

Our efforts during the reporting period were focused on streamlining the operation of the two microreactor units, i.e., Catalytic Microreactor Unit (CMRU) and the Fischer-Tropsch Synthesis Unit (FTSU). The mass flow controllers were recalibrated and the retention times of the different components in the FID and the TCD chromatograms were verified using a standard calibration mixture, in order to ensure the normal operation of the units. These steps were deemed necessary because of the significant downtime experienced by the two units. Runs were initiated towards the end of this period in the CMRU with Fe-Si oxide samples from the University of Kentucky. The results from this investigation will be presented in our subsequent reports.

II. FISCHER-TROPSCH SYNTHESIS ON COBALT CATALYSTS

The kinetic study of Co-based catalysts has continued with the analysis of previously obtained data. Various rate mechanisms were developed capable of describing the observed positive effect of water on the reaction rate. The critical feature common to all these new mechanisms is the existence of multiple parallel pathways for the consumption of CO. For instance:

$CO^* + H^* \rightarrow CH^* + O^*$
$CO^* + H_2O^* \rightarrow COH^* + OH^*$

This postulated mechanism leads to a rate law with two positive terms in the numerator, one of which is first order in H_2O. This type of parallel pathway might explain the puzzling positive H_2O effect that remains, as yet, unexplained. In order to test the validity of such mechanisms, work continues on an efficient computer program capable of fitting the data to the postulated rate laws. Because of the non-linearity of these rates laws, such a program requires minimization over an n-th dimensional error surface; current work focuses on a way to streamline this process in order to minimize computer time.

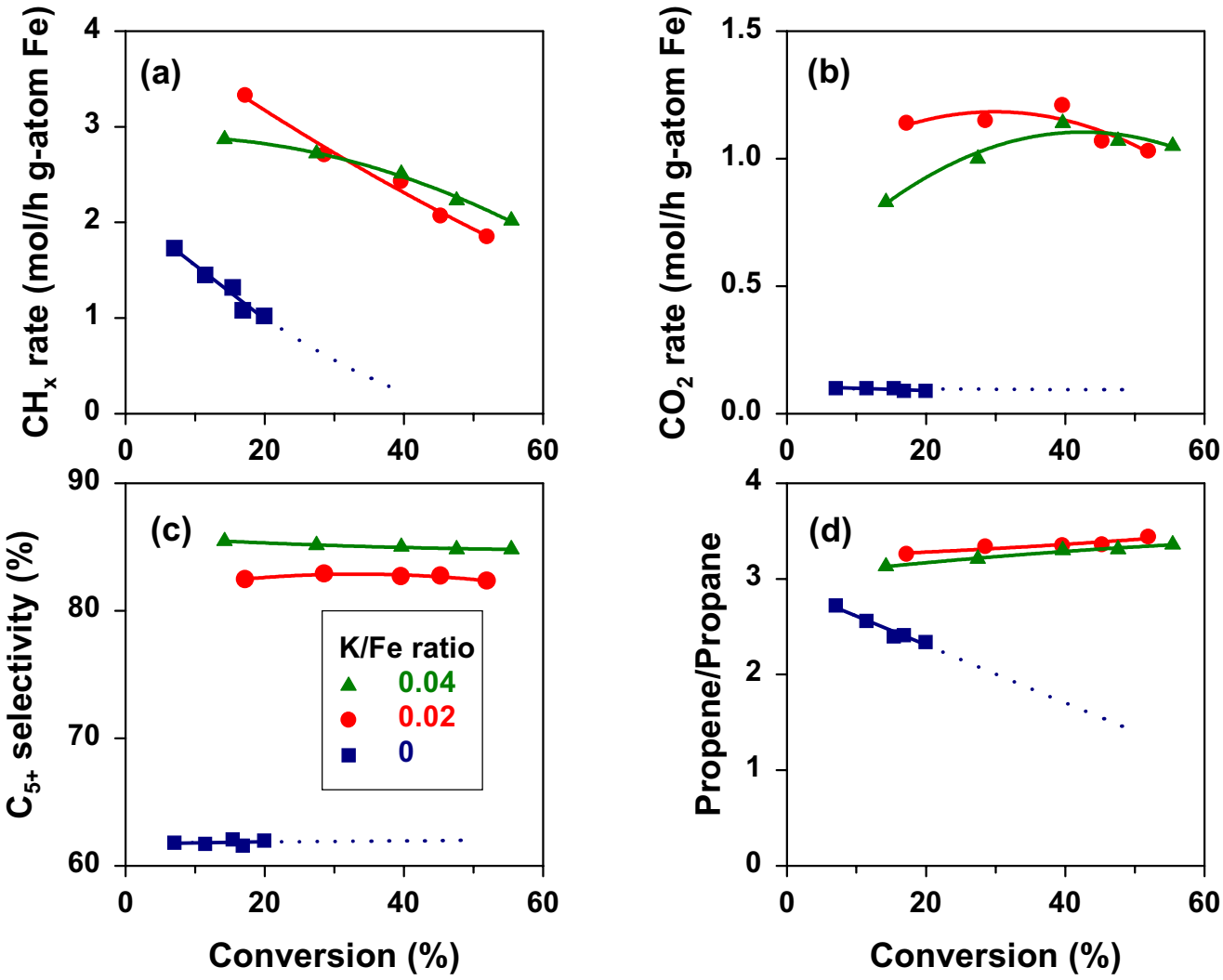

Fig. 1.16 CH_x and CO_2 formation rate, C_{5+} selectivity and propene/propane ratio as a function of CO conversion on the catalyst (0.4g, Cu/Fe=0.01) with varying K loading at 235 ^oC and 21.4 atm in synthesis gas (H_2/CO=2).

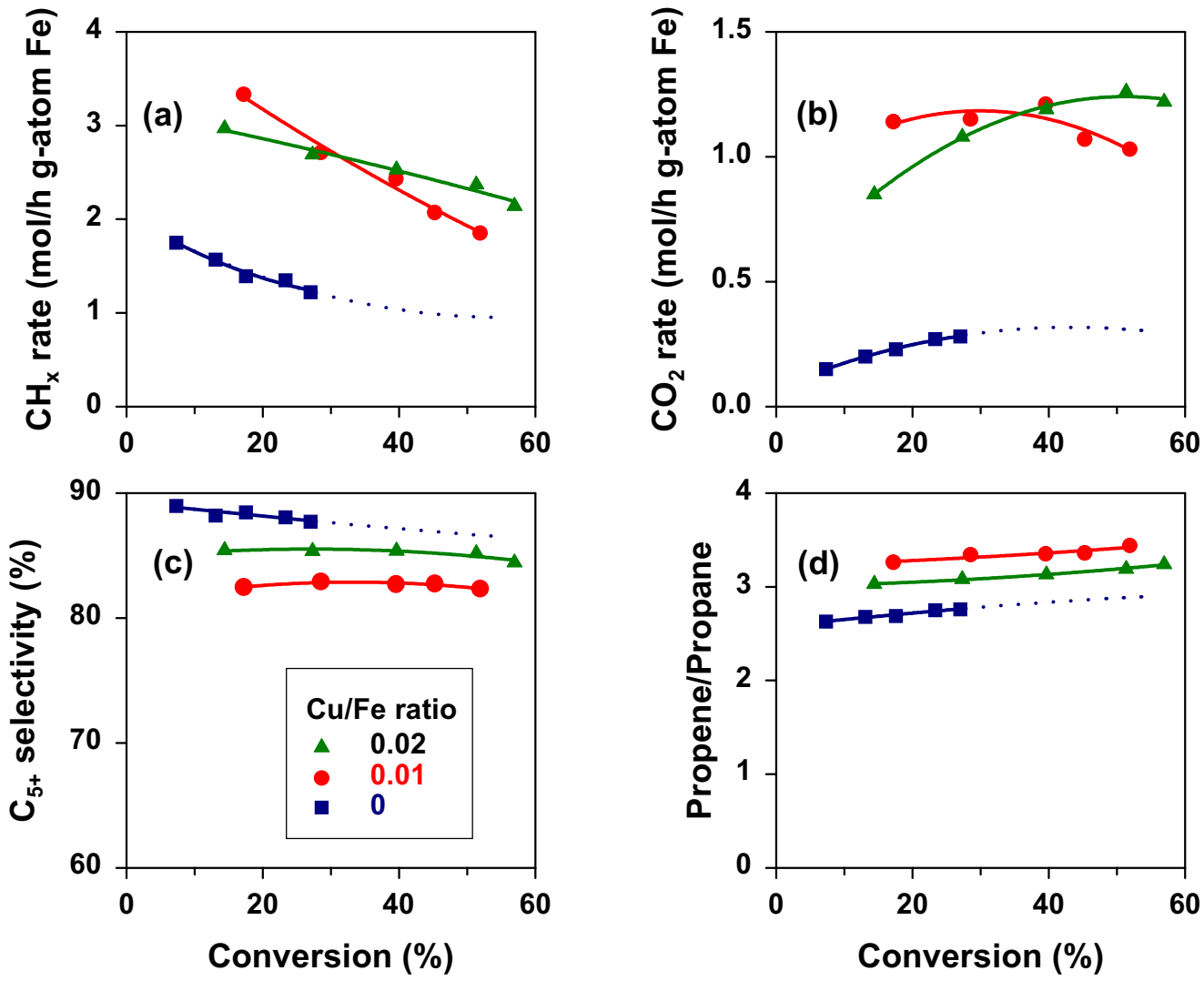

Fig. 1.17 CH_x and CO_2 formation rate, C_{5+} selectivity and propene/propane ratio as a function of CO conversion on the catalyst (0.4g, K/Fe=0.02) with varying Cu loading at 235 ^oC and 21.4 atm in synthesis gas (H_2/CO=2).

II. APPENDIX

1. References

1. M. E. Dry, The Fisher-Tropsch Synthesis, in *Catalysis-Science and Technology*, Vol. 1, p. 160, J. R. Anderson and M. Boudart eds., Springer Verlag, New York, 1981.
2. F. Fischer and H. Tropsch, *Brennstoff-Chem.* **7** (1926) 97.
3. R. B. Anderson, in *Catalysis* Vol. 4, p. 29, P. H. Emmett eds., Van Nostrand-Reinhold, New York, 1956.
4. H. H. Storch, N. Golumbic and R. B. Anderson, *The Fischer-Tropsch and Related Syntheses*, Wiley, New York, 1951; R. B. Anderson, *The Fischer-Tropsch Synthesis*, Wiley, New York, 1984.
5. H. Kolbel and M. Ralek, *Catal. Rev.-Sci. Eng.* **21** (1980) 225.
6. J. W. Niemantsverdriet and A. M. van der Kraan, *J. Catal.* **72** (1981) 385.
7. J. A. Amelse, J. B. Butt and L. J. Schwartz, *J. Phys. Chem.* **82** (1978) 558.
8. G. B. Raupp and W. N. Delgass, *J. Catal.* **58** (1979) 348.
9. R. Dictor and A. T. Bell, *J. Catal.* **97** (1986) 121.
10. J. P. Reymond, P. Meriaudeau and S. J. Teichner, *J. Catal.* **75** (1982) 39.
11. C. S. Kuivila, P. C. Stair and J. B. Butt, *J. Catal.* **118** (1989) 299.
12. C. S. Huang, L. Xu and B. H. Davis, *Fuel Sci. Tech. Int.* **11** (1993) 639.
13. E. Iglesia, and S. C. Reyes, R. J. Madon and S. L. Soled, *Advances in Catalysis*, Vol. 39, p. 221, Academic Press, 1993.
14. E. Iglesia, *Appl. Catal. A: General* **161** (1997) 59.
15. S. Soled, E. Iglesia and R. A. Fiato, *Catal. Lett.* **7** (1990) 271.
16. S. Soled, E. Iglesia, S. Miseo, B. A. DeRites and R. A. Fiato, *Topics in Catal.* **2** (1995) 193.
17. E. Iglesia, A research proposal submitted to the Division of Fossil Energy.
18. D. G. Barton, Ph. D dissertation, University of California, Berkeley, 1998. (XAS cell developed by D. G. Barton, J. A. Biscardi, and G. D. Meitzner)
19. Harold H. Kung
20. Bukur, D. B., Mukesh, D., and Patel, S. A., Ind. Eng. Chem. Res., 29, 194 (1990).
21. Somorjar, G. A., Catal. Rev. Sci. Eng., 23, 189 (1981).
22. 4th Quarterly report, 1998. U.S. Department of Energy under contract # DE-FC26-98FT40308.
23. 1st Quarterly report, 1999. U.S. Department of Energy under contract # DE-FC26-98FT40308.
24. 2nd Quarterly report, 1999. U.S. Department of Energy under contract # DE-FC26-98FT40308.

2. Reaction Cell for *In-situ* X-ray Absorption Spectroscopy Studies

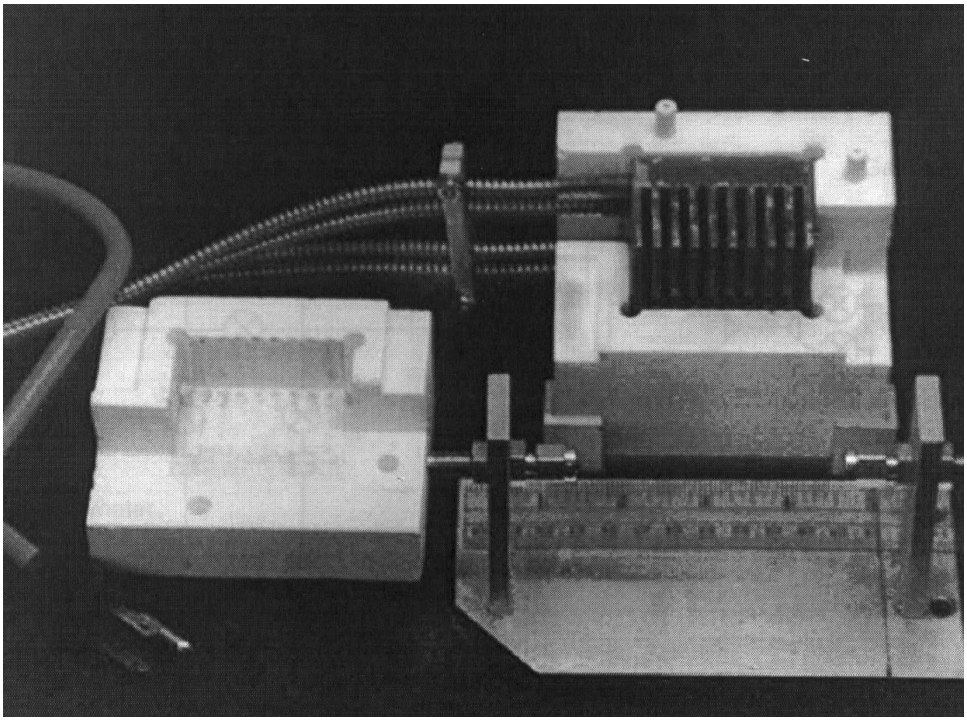

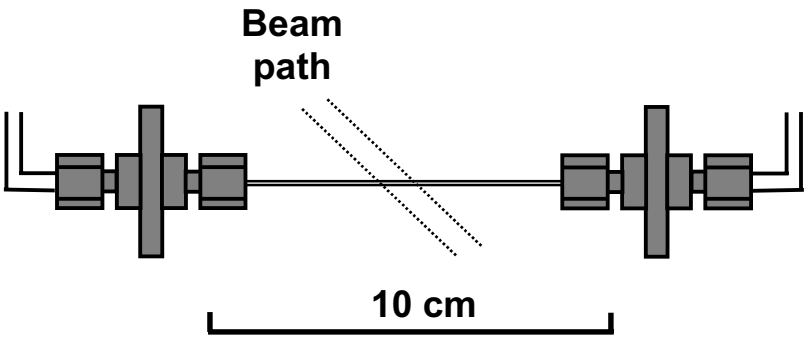

Features:

Small sample: 1-10 mg
Efficient heat transfer: 1 mm capillary
Gas flow rate: 3000-6000 GHSV
Excellent hydrodynamics
Access to reaction conditions: 973 K, 10 atm

Task 12. Reporting/Project Management

Three monthly and one quarterly reports have been completed.